

THE ALPHA MAGNETIC SPECTROMETER ON THE INTERNATIONAL SPACE STATION

ANDREI KOUNINE*

*Laboratory for Nuclear Science, Massachusetts Institute of Technology,
 77 Massachusetts Avenue, Cambridge, MA, USA
 Andrei.Kounine@cern.ch*

Received 17 June 2012

Accepted 20 June 2012

Published 13 July 2012

The Alpha Magnetic Spectrometer (AMS-02) is a general purpose high energy particle detector which was successfully deployed on the International Space Station (ISS) on May 19, 2011 to conduct a unique long duration mission of fundamental physics research in space. Among the physics objectives of AMS are the searches for an understanding of Dark Matter, Anti-matter, the origin of cosmic rays and the exploration of new physics phenomena not possible to study with ground based experiments. This paper reviews the layout of the AMS-02 detector, tests and calibrations performed with the detector on the ground, and its performance on the ISS illustrated with data collected during the first year of operations in space.

Keywords: Cosmic rays; dark matter; anti-matter; space-borne magnetic spectrometer.

PACS Number(s): 26.90.+n

1. Introduction

Significant interest in space-borne particle physics experiments stems from the unique features of experimentation in space, the possibility of studying primordial particles created in the early Universe in an almost background free environment. Success of the first space-borne particle detectors such as IMP-5,^{7,8,1,2} HEAO-3,^{3,4} ACE⁵ and EGRET⁶ lead to more complex experiments, namely PAMELA,^{7,8} FERMI⁹ and AMS-01.¹⁰ These experiments address the most intriguing questions of modern cosmology, specifically the baryon asymmetry of the Universe and its mass density composition.

In addition, there have been many balloon and ground based experiments such as BESS,¹¹ IMAX,¹² HEAT,^{13,14} CAPRICE,¹⁵ WIZARD,¹⁶ Fly's Eye,¹⁷ the

*On behalf of the AMS Collaboration.

P. Auger project,¹⁸ etc. Results of these experiments have and will continue to provide important information on the understanding of the origin of cosmic rays.

AMS-02 is a general particle physics experiment in space. Its purpose is to perform accurate, high statistics, long duration measurements of the spectra of energetic (up to multi-TeV) primary charged cosmic rays. The detector was successfully launched onboard the Space Shuttle *Endeavor* STS-134 mission on May 16, 2011 and deployed on the International Space Station (ISS) on May 19, 2011. Since its activation on ISS, AMS has been and continues to steadily collect data at a rate of 1.4×10^9 events per month. The technical goals of AMS are to reach a sensitivity in the search for anti-matter nuclei of 10^{-10} (ratio of anti-helium nuclei to helium nuclei), an e^+/p rejection of $\sim 1/10^6$ and to measure the composition and spectra of charged particles with an accuracy of 1%. This represents a considerable sensitivity improvement compared to the previous space-borne experiments.

There is a strong demand for precision measurements of cosmic rays in the energy region from 10 to 1000 GeV as the recent measurements of $e^+/(e^+ + e^-)$ by AMS-01, HEAT, PAMELA and FERMI^{19–22} indicate a large deviation of this ratio from the production of e^+ and e^- predicted by a model that includes only ordinary cosmic ray collisions. These available measurements are both at too low an energy and of too limited statistics to shed the light on the origin of this significant excess. AMS-02 is expected to provide definitive answers concerning the nature of this deviation.

2. The AMS-02 Detector

AMS-02 is a general purpose detector to study primordial cosmic ray particles in the energy range from 0.5 to ~ 2000 GeV. In order to ensure that technologies used in the detector construction work reliably in space, a scaled down detector (AMS-01) was built and flown in 1998 onboard the STS-91 mission for 10 days.¹⁰ With this mission it was demonstrated that the AMS experiment can function properly in space. It can withstand the temperature changes from -25° to $+55^\circ\text{C}$ in vacuum, tremendous vibrations (150 dB) and acceleration (3 g) at launch; and its electronics remains fully functional in the harsh radiation environment.

Though the first flight was an engineering flight, over 100 million events were collected. In addition to validating the AMS detector concept, analysis of these events led to the following significant results:

- Search for anti-helium in cosmic rays.²³
- Protons in near earth orbit.²⁴
- Leptons in near earth orbit.²⁵
- Cosmic protons.²⁶
- Helium in near earth orbit.²⁷
- Deuterons in near earth orbit.¹⁰
- Study of trapped and quasi-trapped high energy cosmic rays in near earth orbit.¹⁰
- Positron fraction measurement.²⁸

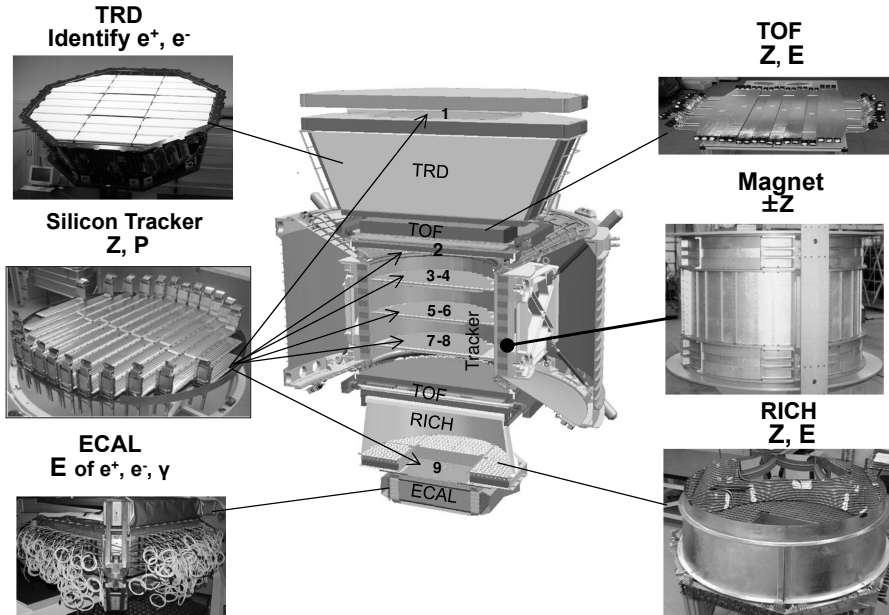


Fig. 1. Schematic view of the AMS detector showing the detector elements and their functions. In AMS particles are identified by their charge (Z), energy (E) and momentum (P). Z and $E \sim P$ are measured independently by the tracker, RICH, TOF and ECAL. In the AMS coordinate system the Y -axis is in the bending direction of the magnet and the Z -axis is vertical.

The layout of the AMS-02 detector for a long duration mission on the ISS is presented in Fig. 1. It consists of a transition radiation detector (TRD); four planes of time of flight counters (TOF); a permanent magnet; a precision silicon tracker; an array of anti-coincidence counters (ACC), surrounding tracker; a ring image Cherenkov detector (RICH); and an electromagnetic calorimeter (ECAL). The electronics consists of 650 microprocessors that reduce the raw data volume by a factor of 1000 without the loss of physics information and downlink the collected data to the ground at an average rate of 10 Mbit/s.

The completed detector measures $5 \text{ m} \times 4 \text{ m} \times 3 \text{ m}$ and weighs 7.5 tons. It has been built to fit within its Unique Supporting Structure which cradles the detector within the shuttle cargo bay for its journey to the Space Station as well as to the attachment point on the Space Station.

2.1. The Transition Radiation Detector

The TRD, is mounted on top of AMS-02 as shown in Fig. 1. It is designed²⁹ to distinguish between light particles and heavy particles of equal charge and momentum, specifically to distinguish between positrons and protons, which give the same signal in the silicon tracker but need to be separated to search for signals from Dark Matter annihilation in the cosmic ray spectra.

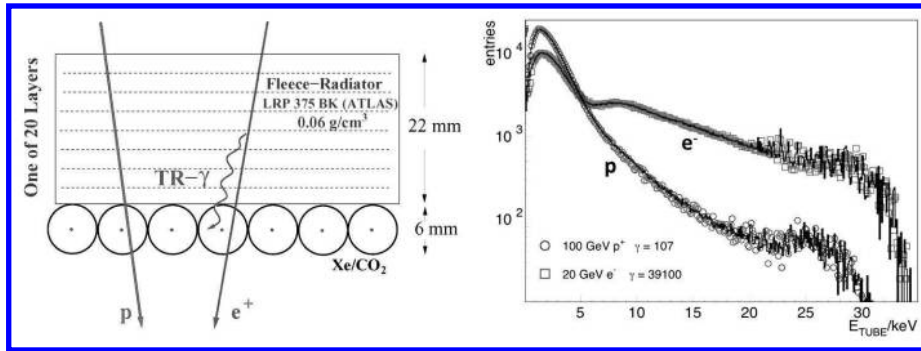


Fig. 2. Detection of ionization losses from charged particles and transition radiation photons in the TRD (left figure) and amplitude spectra of 100 GeV/c protons and 20 GeV/c electrons (right figure) as measured in a dedicated TRD test beam. A significant difference in the shape of the proton and electron spectra is used in the likelihood function to separate these two species in cosmic rays.

The TRD consists of 5,248 straw tubes of 6 mm diameter with a maximum length of 2 m. Sixteen straws are arranged in a module and mounted in 20 layers, each with a fiber fleece radiator of 20 mm thickness. There are 12 layers of straws along the Y -axis (located in the middle of TRD detector) and four plus four layers along the X -axis (located on top and on the bottom of TRD). The assembly of the TRD layers is supported in a tapered octagonal carbon fiber structure, the octagon, with a very low coefficient of thermal expansion. Such a structure ensures the minimum relative movement of the TRD elements with the variation of the ambient temperature. The octagon itself is mounted on the AMS Unique Supporting Structure.

Each straw tube is filled with a Xenon/ CO_2 gas mixture. Xenon efficiently captures the transition radiation generated in the radiator layers. An anode wire in each straw tube captures the signal from the resulting ionization as well as the ionization signal of the traversing charged particle as illustrated in Fig. 2.

The TRD gas system is designed to store, mix and circulate the gas supply for years of TRD operation on the ISS. It consists of a supply and mixing system as well as a circulation system. Operationally, a monthly resupply of approximately 14 g of CO_2 and 46 g of Xenon is used to replace the losses due to diffusion of gas (primarily CO_2) through the straw tube walls. The leak rate of CO_2 was measured to be $5 \mu\text{g/s}$ and this measurement has been stable over years both on the ground and on orbit. With 5 kg of CO_2 and 49 kg of Xenon onboard, this leak rate corresponds to the lifetime of more than 20 years in space.

2.2. The Time of Flight counters

The TOF counters, provide the fast trigger to the experiment, a measurement of particle velocities including discrimination between upward and downward going particles and a measurement of the absolute value of the charge.

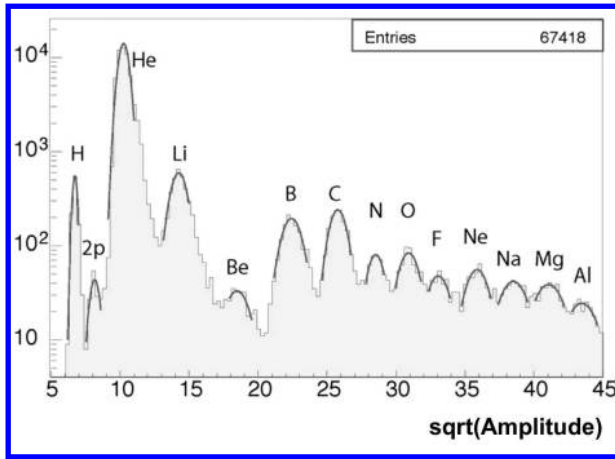


Fig. 3. The square root of the integrated light yield measured by TOF show peaks corresponding to different nuclei. Peak “2p” is produced by two singly charged particles crossing the scintillator at the same time. Be ions were suppressed in this beam.

The TOF design is based on the experience gained with the AMS-01 engineering flight.³⁰ Overall there are four planes of 12 cm wide scintillator paddles oriented in two orthogonal directions. One pair of planes is located above the magnet, the Upper TOF, and another pair is below the magnet, the Lower TOF. Each plane has a sensitive area of 1.2 m². The paddles are overlapped by 0.5 cm within one plane in order to avoid geometrical inefficiencies. They are 1 cm thick, a compromise between minimum thickness requirement and the light output needed to reach the design resolution. Each paddle is instrumented with at least two PMTs at each end.

The system measures energy losses by charged particles and converted photons (to first-order the resulting amplitude is proportional to the square of the particle charge) with a resolution sufficient to distinguish nuclei up to charge $Z \sim 26$. Figure 3 shows the results of the charge measurement by the TOF during an ion test beam.

The average time resolution of each counter has been measured to be 160 picoseconds and the overall velocity ($\beta = v/c$) resolution of the system has been measured to be 4% for $\beta \simeq 1$ and $Z = 1$ particles. The resolution improves with the increase of charge value to reach a limit of $\sim 1\%$ for $Z > 5$ particles.

2.3. The Anti-Coincidence counters

The ACC,³¹ also called the Veto counters, surround the AMS silicon tracker, just inside the inner cylinder of the support structure. Their purpose is to detect events with unwanted particles that enter or leave the inner tracker volume transversely and which could induce signals close to the main particle track such that it could be incorrectly measured, for example confusing a nucleus trajectory with that of an anti-nucleus. The ACC consists of 16 curved scintillator panels of 1 m length,

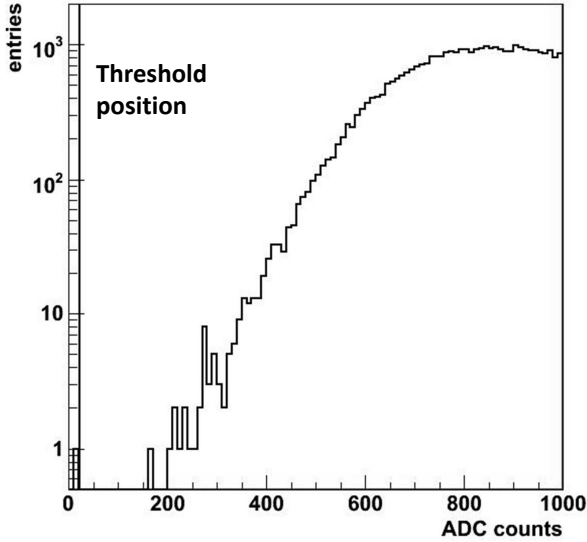


Fig. 4. Efficiency of the ACC measured in a long duration cosmic ray test on the ground. As seen, just 1 in 65,000 particles shows a signal below the threshold.

instrumented with wavelength shifting fibers to collect the light. Collected light is then guided by clear fiber cables to the photomultipliers mounted on the conical flange of the support structure. To maintain the hermeticity of the ACC cylinder, the counters have a tongue and a groove along the vertical edges such that particles crossing this area are detected simultaneously by two panels. As for the TOF, the PMTs are unshielded but positioned with their axes parallel to the local magnetic field. Long duration tests of the counters show they have an efficiency close to 0.99999 as presented in Fig. 4.

2.4. The permanent magnet

The AMS magnet¹⁰ is made of 64 high-grade Nd-Fe-B sectors assembled in a toroidal structure of 1.0 m high and with inner diameter of 1.1 m. This configuration produces a dipole field of 1.4 kGauss in the center of the magnet and negligible dipole moment outside the magnet. This is important in order to eliminate the effect of torque on the shuttle or on the Space Station.

A detailed three-dimensional field map of the magnet was made in 2010 using Hall probes. The field was measured in 120,000 locations to an accuracy of better than 1%. Figure 5 shows some of the results of these measurements. As seen in Fig. 5, the field is almost constant inside but vanishes quickly outside the magnet. Comparison with the measurements performed with the same magnet in 1997, before the engineering flight of AMS-01, shows that the field did not change within 1%, corresponding to the accuracy of the 1997 measurement. This field provides a

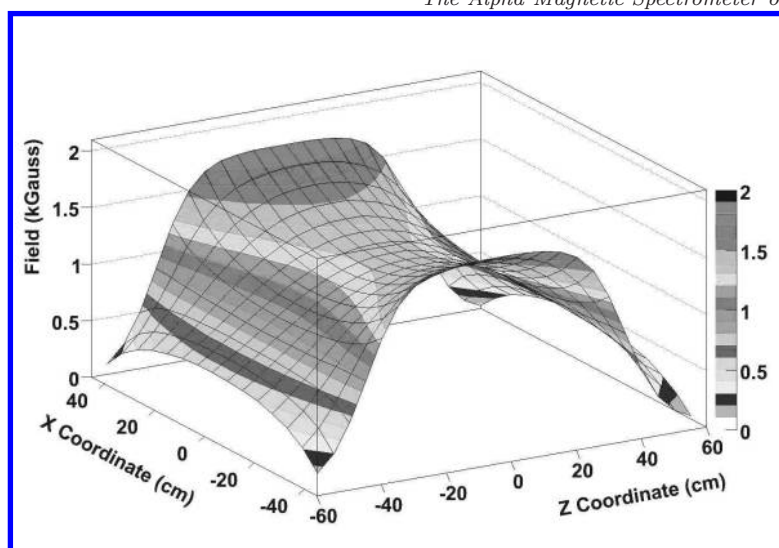


Fig. 5. Results of the 2010 magnetic field measurement in the bore of the magnet over the $X - Z$ plane at $Y = 0$.

bending power sufficient to measure protons up to a Maximal Detectable Rigidity (momentum divided by charge), MDR, of 2.14 TV. For He nuclei the MDR is 3.75 TV.

AMS also developed a superconducting magnet which was suitable for a three year mission on the ISS as originally planned. The superconducting magnet was the same volume as the permanent volume but its field was five times stronger. Using 2500 liters of superfluid helium, the superconducting magnet operated at a temperature of 1.8 K. Many new technologies, such as thermomechanical pumps, persistent switches, cryocoolers, etc., were specifically modified for AMS to ensure its functioning, safety and endurance in space. The superconducting magnet underwent extensive testing with the AMS Detector that validated its performance and endurance in simulated space conditions. These tests also confirmed that the magnet would lose its superconductivity when the superfluid helium boiled off after approximately three years of operation, exactly the length of the mission for which it was originally designed. Because of the retirement of the shuttle fleet, there would have been no means of re-supplying AMS with additional liquid helium.

The superconducting magnet was not used for flight because the lifetime extension of the ISS made the permanent magnet with its extended operational capability and promise of higher yield of data, the instrument of choice. To offset the lower magnetic field of the permanent magnet, the AMS Collaboration optimized the geometry of the detector by adding more silicon planes and rearranging the existing silicon planes and thus greatly increasing the measurement arm. This recovered the full sensitivity for AMS on matter-anti-matter separation as was confirmed with a dedicated beam test.

2.5. The silicon tracker

The tracker is composed of 192 ladders, which is a basic unit that contains the silicon sensors, readout electronics and mechanical support. Three planes of aluminum honeycomb with carbon fiber skins are equipped with silicon ladders on both sides of the plane, numbered from the top 3 to 8 in Fig. 1. Another three planes are equipped with only one layer of silicon ladders. As indicated in Fig. 1, they are located on top of the TRD, plane 1, on top of the magnet, plane 2, and in between the RICH detector and the Electromagnetic Calorimeter, plane 9. Planes 2 through 8 constitute the inner tracker. The goals for this detector are to identify the sign of charged particles, to measure their rigidity and the absolute value of their charge.

Each silicon sensor consists of a substrate of high purity doped silicon 300 mm thick. It has aluminum strips on the two sides of the substrate that run in orthogonal directions. On average, 12 sensors constitute a ladder. Within a ladder strips of different sensors are mechanically aligned with $3 \mu\text{m}$ accuracy. They measure coordinates of charged particles in two orthogonal projections simultaneously. The readout pitch is $110 \mu\text{m}$ in the bending direction and $208 \mu\text{m}$ in the nonbending direction. This granularity provides a coordinate resolution of $10 \mu\text{m}$ in the bending direction³² (Fig. 6). Overall, there are 196,608 readout channels. The signal amplitudes provide a measurement of the particle charge independent of the other detectors (Fig. 6).

To maintain the required resolution of the silicon tracker it is necessary that the positions of the seven layers of the inner tracker be held stable. This mechanical stability is assured by a lightweight, thermally stable carbon fiber structure. It is also monitored using 20 near-UV laser beams which penetrate through all planes of the inner tracker and provide micron level accuracy position measurements.

Though the readout electronics of the tracker has been optimized for low power consumption, the readout of the 200 K channels still dissipates about 144 W inside

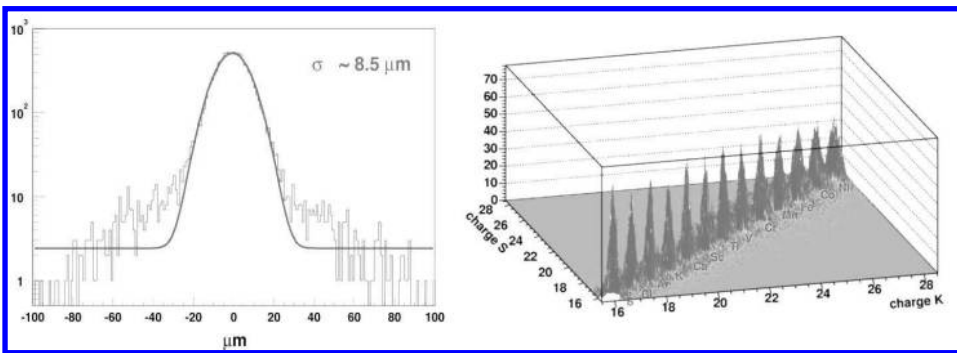


Fig. 6. Performance of the silicon tracker as measured in a dedicated test beam. The left plot shows the coordinate resolution of a single ladder in the bending direction. The right plot shows the correlation of the charges measured by the tracker on the two sides of silicon, denoted S and K .

the magnet. To evacuate this heat the tracker has a dedicated Tracker Thermal Control System. This system maintains the tracker temperature stable within 1°C to ensure stability of pedestals and to minimize the electronics noise.

2.6. The Ring Image Cherenkov Detector

The RICH detector,³³ is designed to distinguish between isotopes in cosmic rays by measuring the velocities of charged particles with a precision of one part in a thousand. The detector consists of a two dielectric radiators that induce the emission of a cone of photons when traversed by charged particles with a velocity greater than that of the phase velocity of light in the material. In the center are 16 tiles of 5 mm thick sodium fluoride, with a refractive index $n = 1.33$. The central radiator is surrounded by 92 tiles of 25 mm thick silica aerogel, with a refractive index $n = 1.05$. This allows detection of particles with velocities $\beta > 0.75$ (for the sodium fluoride) and $\beta > 0.953$ (for the silica aerogel). The emitted photons are detected by an array of 10,880 photon sensors with an effective spatial granularity of $8.5 \times 8.5 \text{ mm}^2$ at an expansion distance of 45 cm. To reduce lateral losses the expansion volume is surrounded by a high reflectivity reflector with the shape of a truncated cone.

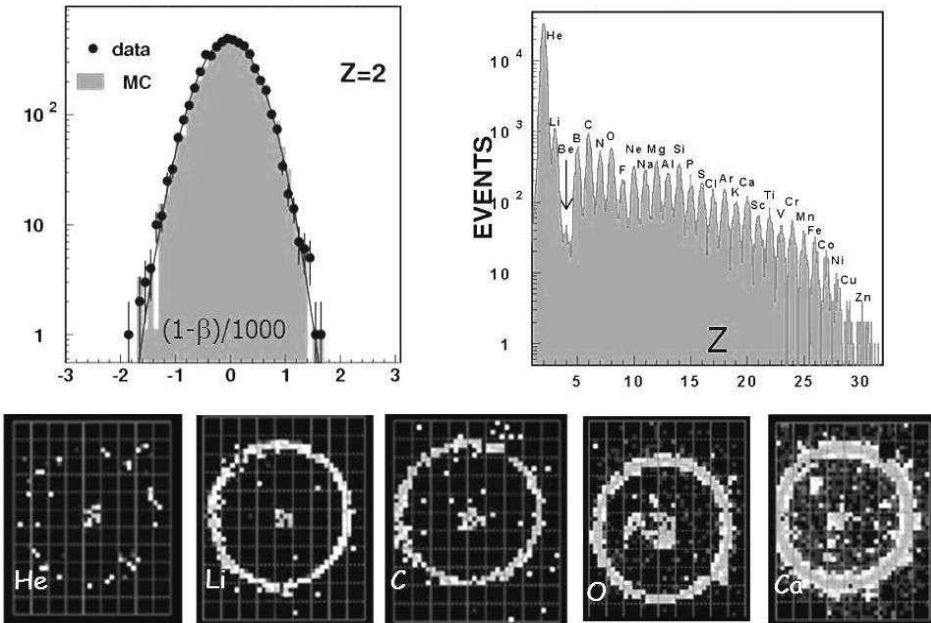


Fig. 7. Results of the RICH ion test beam. The top left plot demonstrates that the accuracy of the velocity measurement for He nuclei is 1/1000. The top right plot shows that all ions available in the beam can be identified. Along the bottom individual event displays are presented. The beam was Be suppressed.

Cherenkov radiation is emitted when a charged particle travels through a dielectric medium with a speed greater than that of light in the same medium. The particle emits radiation along a cone of light as it passes through the thin radiator of the RICH detector. Given the refractive index of the radiator, the opening angle of the radiation cone provides a direct measurement of the velocity of the incoming charged particle. By counting the number of emitted photons the charge squared (Z^2) of the particle can be determined. Test beam results from the RICH at $E = 158$ GeV/n are shown in Fig. 7 and indicate that velocity can be measured to an accuracy of 1/1000 and, simultaneously, nucleons can be identified up to Cu, $Z \sim 30$.

2.7. The Electromagnetic Calorimeter

The ECAL,³⁴ consists of a multilayer sandwich of lead and scintillating fibers with an active area of 648×648 mm² and a thickness of 166.5 mm. The calorimeter is composed of 9 superlayers, each 18.5 mm thick and made of 11 grooved, 1 mm thick lead foils interleaved with 10 layers of 1 mm diameter scintillating fibers. In each superlayer, the fibers run in one direction only. The three-dimensional imaging capability of the detector is obtained by stacking alternate superlayers with fibers parallel to the X and Y axes (5 and 4 superlayers, respectively). The calorimeter has a measured thickness corresponding to 17 radiation lengths.

All fibers are read out on one end by 324 photomultipliers. Every photomultiplier has four anodes and is surrounded by a magnetic shield which contains light guides, the PMT base and the front end electronics. Each anode covers an active area

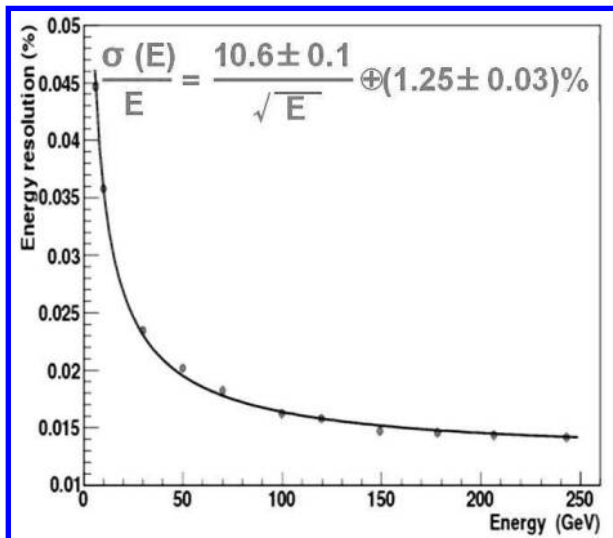


Fig. 8. Results of a dedicated beam test with the ECAL. The ECAL energy resolution for electromagnetic showers is measured as a function of the beam energy. Parametrization of this dependence is also indicated.

of $9 \times 9 \text{ mm}^2$, corresponding to about 35 fibers, defined as a cell. In total the ECAL is subdivided into 1296 cells and this allows a sampling of the longitudinal shower profile by 18 independent measurements. The signals are processed over a wide dynamic range, from one minimum ionizing particle, which produces about 8 photoelectrons per cell, up to the 60,000 photoelectrons produced in one cell by the electromagnetic shower of a 1 TeV electron. The ECAL performance was studied in high energy electron and proton beams. The energy resolution for high energy electrons is measured to be 1.5–3% (see Fig. 8), the angular resolution is $\sim 1^\circ$ and the e/p separation is estimated to be better than 500 for energies above 100 GeV. Combined with the momentum information from the tracker (energy–momentum matching), e/p separation reaches $\sim 10^4$ level.

2.8. The star trackers and GPS

The physics scope of AMS-02 is greatly broadened by the measurement of gamma rays, for which the measured direction indicates their point of origin. In order to correlate the directional measurements of AMS with galactic coordinates, a pair of small optical telescopes are mounted on each side of the inner tracker. They acquire the images of the stars, which are compared with those in an astrometric star catalogue. With this information, the orientation of AMS can be determined within an accuracy of a few arc seconds.

In addition to the directional correlation provided by the star tracker, the physics accessible by measuring gamma rays also requires the precise, to a few microseconds, temporal correlation of measurements by AMS-02 with other experiments. Timing information is provided by the Space Station, but owing to the limitations of the ISS electronics and the processing required within AMS, the reference time accuracy would be about 100 msec. To improve on that the AMS detector is equipped with a global positioning system (GPS). This allows AMS to assign an accurate (with a precision of $\sim 1 \mu\text{s}$) time stamp for every collected event.

2.9. The electronics

The electronics comprise 650 processors, which perform acquisition of the physics data and permanently monitor the state of the detector (Fig. 9). Interconnectivity of all the elements is provided by high speed serial links, AMSWire, for physics data acquisition and conventional Controller Area Network (CAN) buses for monitoring and control. The system also has several interfaces to the Space Station and the Space Shuttle, including those for power, for commanding and monitoring (the Low Rate Data Link, LRDL) and for data downlink (High Rate Data Link, HRDL).

For the design of the electronics, AMS has taken the high performance technologies used in particle physics and implemented them for use in low Earth orbit. A unified approach has been made to meet all the requirements imposed by the different AMS detectors, by NASA and most importantly, by the physics goals. Particular

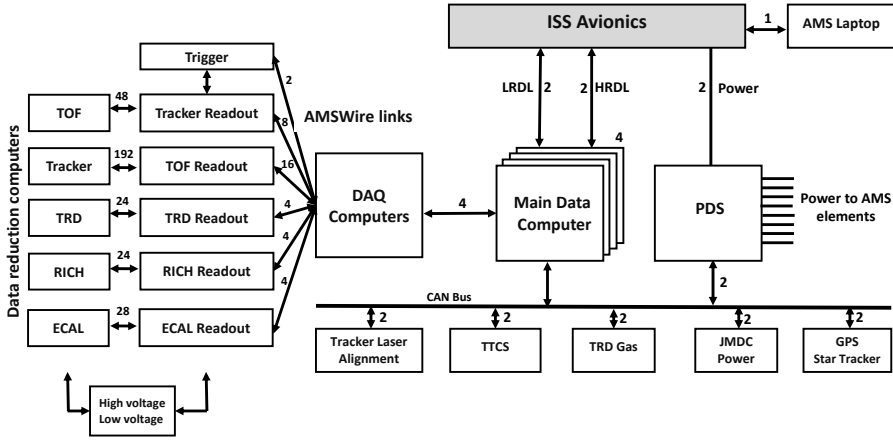


Fig. 9. Block diagram of the AMS electronics. Data acquisition, monitoring and command interfaces to NASA are shown. The number of computers in the detector specific branches of the DAQ tree and on the CAN buses, including those redundant, is also indicated.

effort has been made to ensure that the data acquisition and trigger electronics will meet the performance requirements for decades of on orbit operations.

Computers performing the data acquisition, DAQ, form a tree-like structure. There are 272 data reduction computers (typically double redundant) connected to the front end electronics which perform digitization of incoming signals, subtract pedestals, remove empty channels, format events and send them to the next level. There 28 readout computers (all double redundant) receive the information, assemble it and send it to the next level. These computers also distribute trigger signals and collect busy signals and are used to control low and high voltages in the detectors and to distribute commands. Two redundant trigger computers generate AMS triggers and control busy signals. They also format trigger-related information and send it to the next level. Four redundant DAQ computers collect all the information from the lower levels, format it and send to one of the four redundant main data computers. DAQ computers also distribute commands to the lower levels. All these nodes are all interconnected with custom designed AMSwire serial links with a throughput of 100 Mbit/sec.

Monitoring and control of the experiment is ensured by 12 double redundant computers connected *via* CAN buses to the main data computers. These computers collect information and control the tracker laser alignment system, the Tracker Thermal Control System, the TRD gas system, the AMS power distribution system, the Star Trackers and the GPS as well as 1118 temperature sensors and 298 heaters.

Power on the ISS comes from the eight large solar arrays. AMS has two power feeds, each connected to one of the arrays. The power is provided at voltages ranging from 109 to 126 VDC. The AMS power distribution system efficiently converts up to 2500 W at this voltage to the 28 VDC used in AMS. It is also equipped with

a thermal interlock which diverts power into heaters whenever AMS is turned on until the system temperature is within its operational range.

The LRDL is based on the MIL-STD 1553B dual serial bus, widely used in aircraft. The main data computers are connected to these buses, with only one selected to actively manage this link by a command from the ground. There are two redundant connections from AMS to these buses that can be interchanged by an astronaut during an extra-vehicular activity.

The HRDL is the main AMS data downlink channel. It is based on a NASA specific implementation of TAXI fiber optic communications. The link can move data on the ISS at speeds up to 90 Mbit/sec. Of this AMS has been allocated an orbit average of 10 Mbit/sec to downlink collected data to the ground. Again, there are two redundant connections from AMS that can be interchanged by an astronaut during an extra-vehicular activity.

In addition to the electronics mounted on the AMS detector, there is a dedicated computer, the AMS Laptop (also shown in Fig. 9), located in the pressurized compartment of the ISS. This computer provides the primary backup for AMS data (it can store 2 months of AMS data) as well as an alternate command route from the ground to AMS.

2.10. Thermal system

The thermal environment on the ISS is constantly changing. To ensure that components operate within safe thermal limits, AMS is equipped with 1118 temperature sensors, radiators and 298 thermostatically controlled heaters. Heavy use is made of insulating shims between structural members and of multi-layer insulation between different volumes to maintain thermal separation and to avoid uncontrolled heat flow. Heat is always conducted to radiators, while minimum operating temperatures are maintained by thermostatically controlled heaters. Two vital elements, the main data computers and the power distribution system, are also equipped with thermal interlocks, which divert power into heaters until the corresponding temperature is within the operational range.

The electronics dissipates up to 1500 W, a significant heat load that must be directed away from the detectors. Therefore most of the electronics boxes are mounted directly on the two 4 m² main radiators located on the opposite sides of AMS centered on the $\pm Y$ axes but called wake and ram with reference to the usual ISS direction of travel. Ammonia heat pipes embedded within the radiators ensure the transfer of the heat evenly over the entire area of the radiator. Radiation back towards the detectors and support structure is blocked by surface treatment of the inner radiator surfaces and multi-layer insulation around the electronics boxes.

The Tracker Thermal Control System (TTCS), keeps the tracker front end electronics temperatures stable within 1°C to ensure its optimal performance. To evacuate the heat dissipated by the tracker front end electronics inside the magnet bore, the heat dissipating elements are thermally connected by bars to two cooling

loops filled with high pressure liquid CO₂. The CO₂ absorbs the heat and boils. It is then mechanically transported to radiators to release excess of the heat and condense. This system uses 142 temperature sensors, four pressure sensors, four pumps and 32 heaters as well as two dedicated radiators.

2.11. Trigger and data acquisition system

The acquisition of physics data in the electronics is driven by the trigger system, which ensures synchronous operations of the entire DAQ tree. One of the two redundant trigger computers collects inputs from the TOF, Veto and ECAL, combines them according to various physics goals and distributes a trigger signal to all the detectors to start their readout cycles. There are seven types of triggers in AMS, each one dedicated to a specific physics channel. This includes triggers for charged particles, ions, strangelets, electrons and positrons, photons as well as two prescaled unbiased triggers to aid in calculating efficiencies for triggering on charged and electromagnetic particles. The total trigger rate varies from 200 to 2000 Hz, depending on the geomagnetic latitude.

The data acquisition system is designed to operate at trigger rates up to 3000 Hz. Optimization of the system in terms of processing time, link throughput, event size and the amount of buffering at each DAQ level was performed at the maximal expected particle rate on orbit of ~ 2000 Hz (Fig. 10). At this rate the raw data volume is 7 Gbit/sec. Extensive data reduction is performed in parallel in the 272 data reduction computers to reduce this data volume to the average 10 Mbit/sec allocated to AMS by NASA. Event buffering is introduced at every level of the DAQ tree to optimize the performance of the overall system, event processing time is kept below 300 μ s at all levels of the DAQ tree and the reduced average event size is

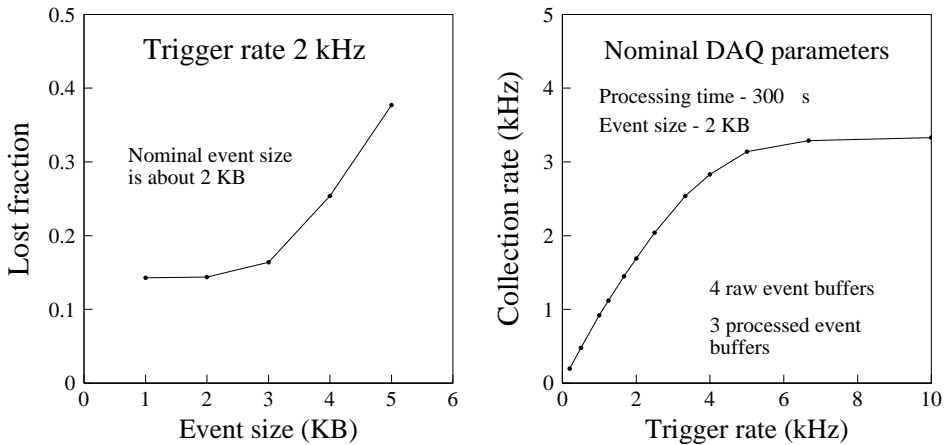


Fig. 10. Optimization studies of the AMS data acquisition system. The left plot shows the data acquisition inefficiency as a function of the average event size. The right plot shows the rate at which particles can be collected as a function of the input trigger rate.

around 2400 bytes for the data collected on orbit. In order to address Single Event Effects, in particular bit flips due to radiation in memory of the various electronics components, each event fragment is protected with a 16-bit CRC code.³⁵

In the readout and DAQ computers the data from the data reduction computers are collated, buffered and then sent to the main data computer which receives the complete event, analyses it for integrity and performs lossless data compression based on the Huffman encoding.³⁶ The compressed data are buffered in 112 gbyte of flash memory and down-linked to the ground whenever the connection is available.

3. Detector Qualification Tests

Each AMS subsystem has been subjected to a rigorous series of space qualification tests. These include thermal, vibration, electromagnetic compatibility and Thermal-Vacuum (TV) tests as well as studies with electron, proton and ion beams. In addition, several system wide tests were performed with the integrated experiment including test beams at CERN as well as electromagnetic compatibility and TV tests at the European Space Research and Technology Center, ESTEC, in Holland.

3.1. Selection of components and production process

To meet the performance requirements, the electronics primarily uses high grade industrial components and achieves reliability by interconnecting redundant elements. Rigorous screening of the components and extensive testing during design and production processes ensure that desired reliability is indeed achieved.

To ensure that electronics will operate properly in space, a process has been developed leading from iterations of circuit design and component selection through mechanical design and material selection to the production, quality assurance and space qualification of a series of models. Candidate components are used to implement prototype circuits to verify the design principles. After a few iterations, this leads to engineering models (EM), which are functionally equivalent to the flight boards. The EM are then reimplemented using high reliability components into a series of Qualification Models (QM), which pass through extensive testing including vibration and thermal cycling at the board level and also TV and electromagnetic compatibility tests at box level. Test levels are well beyond those expected in flight. The goal of all these tests is to verify the reliability of individual components as well as to establish the production process. The flight models and flight model spares (FM, FS) are produced and qualified with thermal cycling, vibration and TV tests to the levels expected in flight, ensuring that each performs within requirements. Figure 11 shows the temperature profile of the TV test of the QM of the main data computers. Pressure in the chamber was kept below 10^{-5} mbar during the test. Successful functional tests were performed at -25°C and at $+55^{\circ}\text{C}$, 5°C beyond the limits of the operational range.

The key aspect in this process is the selection of electronics components, especially those either resistant to, or tolerant of, Single Event Effects in the harsh

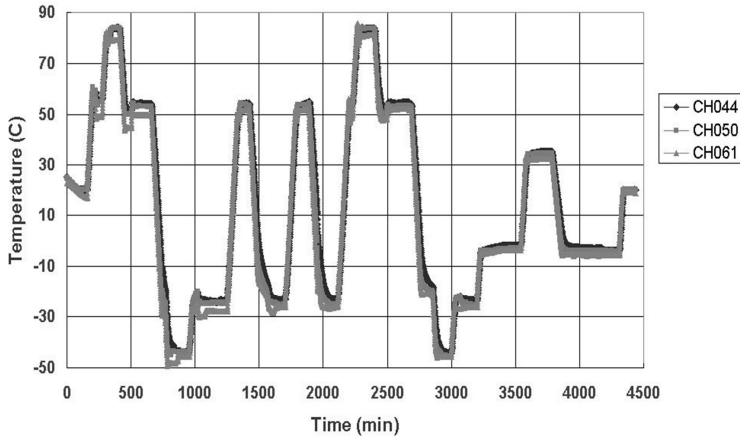


Fig. 11. Thermal-vacuum space qualification test of the QM main data computers. Functional tests were performed at -25°C and at $+55^{\circ}\text{C}$. At the extremes of the nonoperational temperature range (-45°C to $+85^{\circ}\text{C}$) the computers were powered off. All the tested temperature extremes were intentionally extended by 5°C compared to the on-orbit requirements.

radiation environment on orbit. Several tests with heavy ion beams were performed on electronics components. Only 60% of all tested components were retained for use.

3.2. The electromagnetic compatibility test

The AMS experiment underwent an electromagnetic compatibility test in the large Maxwell test chamber at ESTEC in February and March 2010. The objectives of this test were to verify that the performance of the detector will not be adversely affected by the expected electromagnetic environment of the Shuttle or the Station and to verify that AMS will not generate electromagnetic interference that will adversely affect either vehicle. Each of the electronic subsystems designs had previously been successfully tested at box level. This testing of the complete detector was required as part of the NASA safety verification of AMS. Both conductive and radiative tests were performed. In general AMS was well within acceptable limits. As an example, measured conductive emission of AMS on the positive power line is presented in Fig. 12. For the only three slight exceedances in radiative emission at 10 KHz, 7 MHz and 400 MHz, NASA waivers were obtained.

3.3. Thermal Vacuum Test

A TV/Thermal Balance (TB) test was performed in the Large Space Simulator chamber at ESTEC in March and April 2010. The main objectives of the test were to test the performance of the integrated detectors under vacuum in a wide range of temperatures close to those expected on the Space Station, verification of the operability and the performance of the thermal control system and verification of

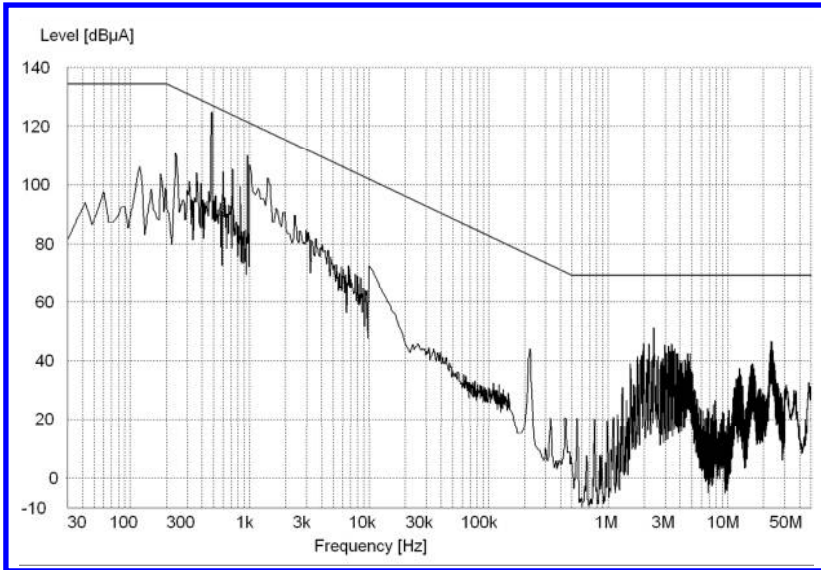


Fig. 12. Conductive emission of AMS on the positive power line. The solid straight line represents the limits set by NASA.

the thermal model. In particular, the heat rejection capability of the radiators was verified. This is a very different mechanism compared to the convective cooling which occurs during tests on the ground in ambient conditions. The TV/TB test at the system level was required to verify the integrated performance of the experiments. The functionality of heaters and thermal interlocks was verified, including their impact on the overall AMS power consumption.

Two functional tests were performed emulating routine operations on orbit. The first was with the chamber wall temperature set to -90°C and an average AMS temperature -21°C . The second was with the chamber wall temperature set to -30°C and an average AMS temperature -12°C . During these tests AMS was collecting cosmic ray data, which were used to monitor performance of each of the detectors when varying the thermal environment.

4. AMS Detector Calibration

In order to produce physics results several types of calibrations are applied to collected data. Absolute energy and momentum scales are established for each detector using particle beams in dedicated tests on the ground. To ensure long term stability of these absolute scales in varying environment, corrections are applied to data. These corrections are determined using specific samples of particles. In addition, during nominal detector operations, stability of electronics response is ensured by frequent, every 30–40 min, calibrations of all electronic channels.

4.1. Test beam calibration

AMS was placed in a CERN test beam and exposed to 400 GeV protons, 10–290 GeV electrons and 10–180 GeV pions from 8–20 August 2010. The AMS detector was installed on a support structure which allowed 2 axes of translation and 2 axes of rotation for exposure to particles from all directions, as in space. Figure 13 summarizes the results from the data collected in the test beam by the integrated detector, showing that the track coordinate resolution is $10\ \mu\text{m}$ [Fig. 13(a)], the energy resolution for electrons is 2.5 to 3% [Fig. 13(b)], the velocity resolution of the RICH is 1/1000 with 400 GeV protons [Fig. 13(c)] and that, for 400 GeV protons, the TRD provides a proton rejection factor of 1/120 at 90% electron selection efficiency [Fig. 13(d)]. The combined proton rejection factor of the TRD and the ECAL at 400 GeV was measured to be 10^{-6} , as designed.

4.2. Calibration with cosmic muons

During processing of the experiment for the Shuttle flight and operations on the ISS at Kennedy Space Center, KSC, from September 2010 to March 2011, data were routinely collected to check the performance of the detectors using sea level cosmic rays. Most of calibration procedures and other routine detector procedures were verified during this period. In addition, the command, data and power interfaces

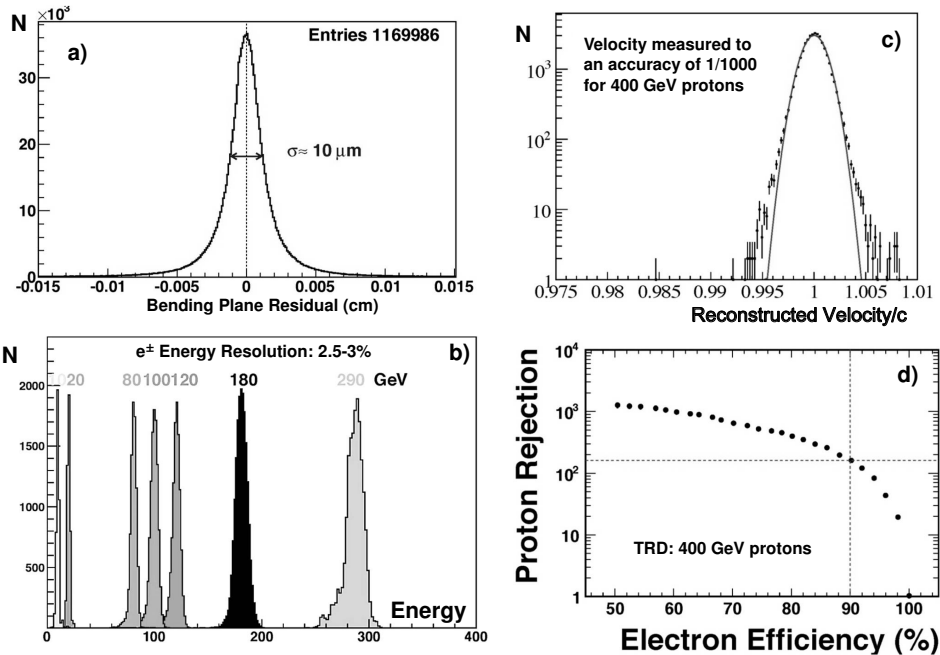


Fig. 13. Summary of the beam test results: (a) Tracker coordinate resolution; (b) ECAL energy resolution; (c) RICH velocity resolution; (d) TRD e/p separation.

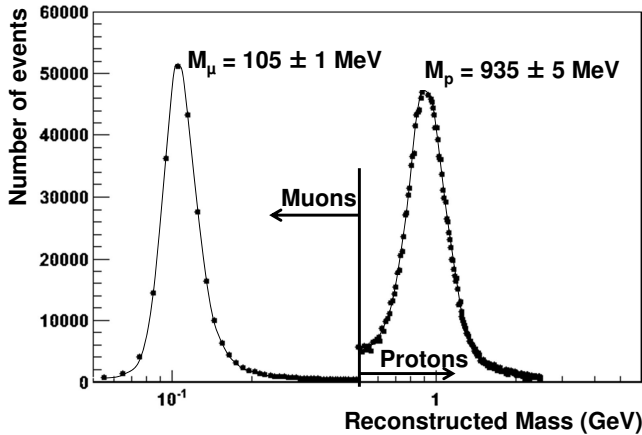


Fig. 14. Reconstructed masses of cosmic ray muons and protons (KSC data).

to the Shuttle and ISS were verified, as for these tests only flight commanding and data interfaces were used. Physics performance during these tests was excellent as demonstrated by Fig. 14 which shows the reconstructed masses of cosmic ray muons and protons collected at KSC.

4.3. Calibration of the detector in space

AMS was installed on the ISS on May 19, 2011 and since then the experiment has been and continues to collect data at an average rate of 10 Mbps. Particle rates over one ISS orbit vary between 200 Hz near the equator to about 2000 Hz near the Earth's magnetic poles. The data acquisition efficiency is on average 85% (it reaches 96% near the equator and 65% near the poles) resulting in an average event acquisition rate of ~ 600 Hz. Over 17 billion events have been collected during the first year of operations in space (Fig. 15). Over its lifetime of 20 years, AMS will collect over 300 billion events. This will provide unprecedented sensitivity to search for new phenomena.

The status of all subsystems is constantly monitored by the AMS shifts. There are around five to twelve physicists on shift at any given time in the AMS Payload Operations and Control Center, POCC, at CERN. Dynamically changing parameters (data downlink bandwidth, distribution of available electrical power, rotation of ISS solar panels and radiators near AMS, etc.) are followed by the operators, who are in permanent contact with NASA ground personnel on voice loops. Commands are sent to AMS from the POCC in response to changing conditions, as necessary.

All subsystems are fully operational with the performance expected from ground measurements. To account for the ever changing environmental conditions, an onboard calibration of all detectors is performed every 42 min (corresponding to half of an ISS orbit). This calibration ensures electronics stability by measuring pedestals and noise levels for all the electronics channels.

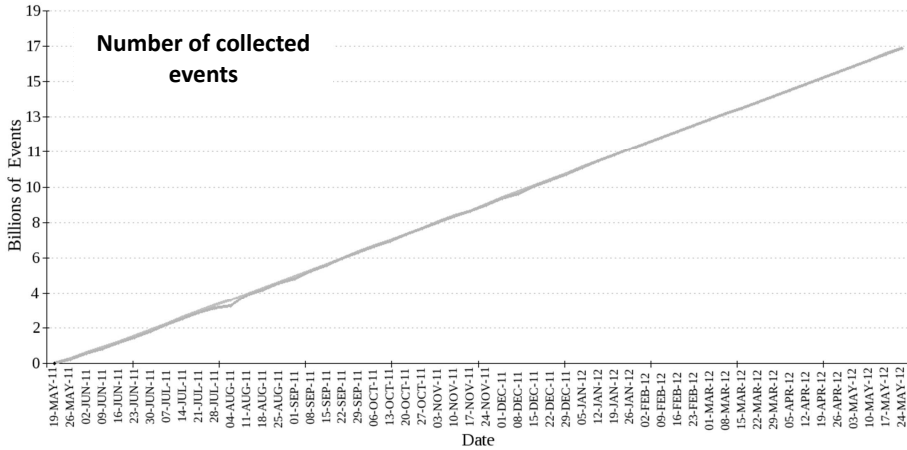


Fig. 15. Over 17 billion cosmic rays have been collected during the first year of operation on the ISS.

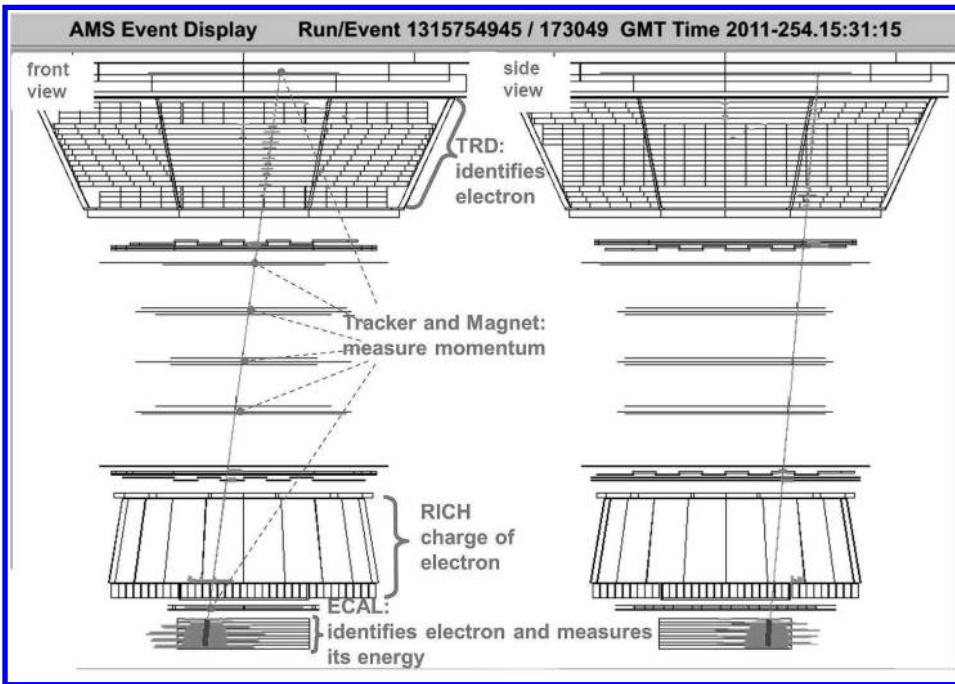


Fig. 16. Example of a high energy electron event collected by AMS on the ISS.

In order to maximize the accuracy of the measurements, variations of ambient conditions, in particular the thermal environment, are accounted for using several advanced calibrations. These calibrations are regularly performed during the off-line data processing for every set of newly collected data. They include gain corrections

for the TRD, TOF, RICH and ECAL, alignment of the tracker planes, alignment of the TRD and the ECAL, etc.

An example of a high energy electron event collected by AMS on the ISS (with all calibration corrections applied) is presented in Fig. 16. The reconstructed particle track extends from the tracker plane on top of the TRD, through the TRD, the upper TOF, the inner tracker planes in the bore of the magnet, the lower TOF, the RICH, the tracker plane on top of the ECAL and into the ECAL. The measured rigidity (-711 GV) of the track indicates this is a particle with negative charge. Pulse heights from the TRD, flag this cleanly as an electron (or positron). Times measured in the TOF indicate it is a downward going particle. Signals in the RICH correspond to a particle of unit charge as do the dE/dx depositions in the TOF and tracker. Finally, the shower shape and size measured by the ECAL identifies this as an electromagnetic particle with a shower collinear with the particle track and an energy of 1.03 TeV.

5. AMS Physics Potential

AMS-02 is a general purpose particle detector capable of simultaneously identifying and measuring all cosmic ray particle species: photons, electrons, protons and nuclei as well as all corresponding anti-particles. This feature becomes very important for distinguishing signals from new phenomena and background processes, given a significant uncertainty in the background calculations related to the modeling of the standard processes and subsequent propagation. AMS will measure spectra for nuclei in the energy range from 0.5 GeV/nucleon to 2 TeV/nucleon with 1% accuracy over the 11-year solar cycle. These spectra will constitute a stringent experimental

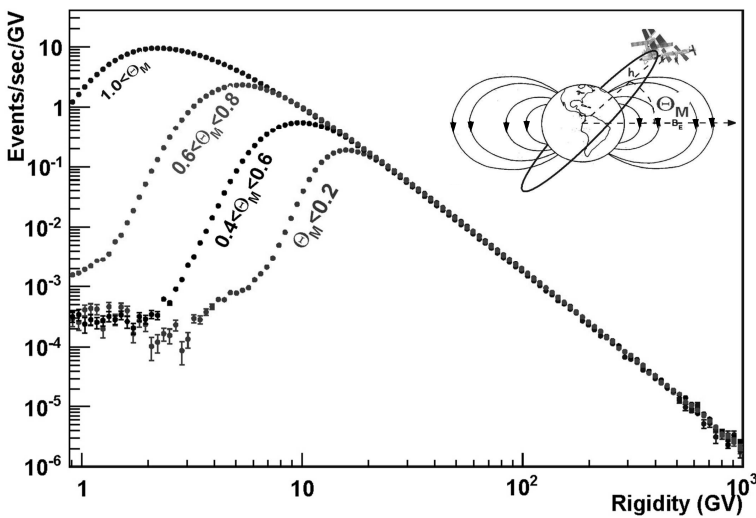


Fig. 17. The rate of helium nuclei as a function of measured rigidity at different geomagnetic latitudes.

test of the assumptions that go into the background estimates. As an example, the helium rate measured at different geomagnetic latitudes is presented in Fig. 17, which shows the effect of the geomagnetic cutoff as well as the presence of the under-cutoff spectrum, an effect already reported by AMS-01.¹⁰

5.1. Search for dark matter

The most appealing candidate for Dark Matter is a stable neutralino.³⁷ It is a generic ingredient of SUSY models with a breaking scale of a few hundred GeV. AMS-02 has potential to study neutralino annihilation simultaneously using four different final state particles: positrons, anti-protons, anti-deuterons and photons. The available low energy measurements of the positron fraction^{19–22} indicate a strong deviation from the estimates based on the model that takes into account only cosmic ray collisions. AMS-02 will measure all nuclei spectra thus providing stringent constraints on the background estimates. It is also important to extend the energy range of the measurements to the TeV range in order to assess any changes in the behavior of the positron fraction at energies up to 1 TeV. This is one of the primary goals of AMS.

Positrons produced in the annihilation of Dark Matter in the galactic halo present one of the most interesting channels for Dark Matter searches. The main background to this measurement is protons. In order to achieve a background rejection of 10^{-6} , AMS uses the identification of electrons and positrons in the TRD (above the magnet) and ECAL (below the magnet) on an event by event basis. The sign of the charge is identified by the fit of the track curvature in the magnet.

As an example of this identification, Fig. 18 shows the log likelihood estimator from the TRD used to separate protons from positrons or electrons. As seen in this figure, at an e^{\pm} efficiency of 90%, the rejection power approaches a factor of 10,000 in the energy range from 3 to 100 GeV.

Figure 19 shows the ECAL estimator, Boosted Decision Tree, used to separate protons from positrons or electrons by analyzing the shower shape. As seen in this figure, at an e^{\pm} efficiency of 90%, the rejection power of ECAL is ~ 400 in the energy range from 3 to 1000 GeV. When the loose energy–momentum matching ($E/P > 0.5$) is included the rejection factor reaches 5000. It should be noted that, at present, these numbers are being improved using refined reconstruction techniques.

Figure 20 shows four high energy positron events. These are examples of highest energy cosmic ray positrons ever measured directly. To illustrate the power of high statistics data samples that will be collected by AMS over its life span in the ISS, Fig. 21 shows the dependence of the expected shape of the positron fraction on the neutralino mass. The simulated structure in the spectrum due to the contribution of Dark Matter collisions is distinct up to neutralino masses of 1 TeV. A large data sample expected from 18 years on ISS along with the good energy resolution of 2% implies that should this enhancement have a structure it can be clearly seen.

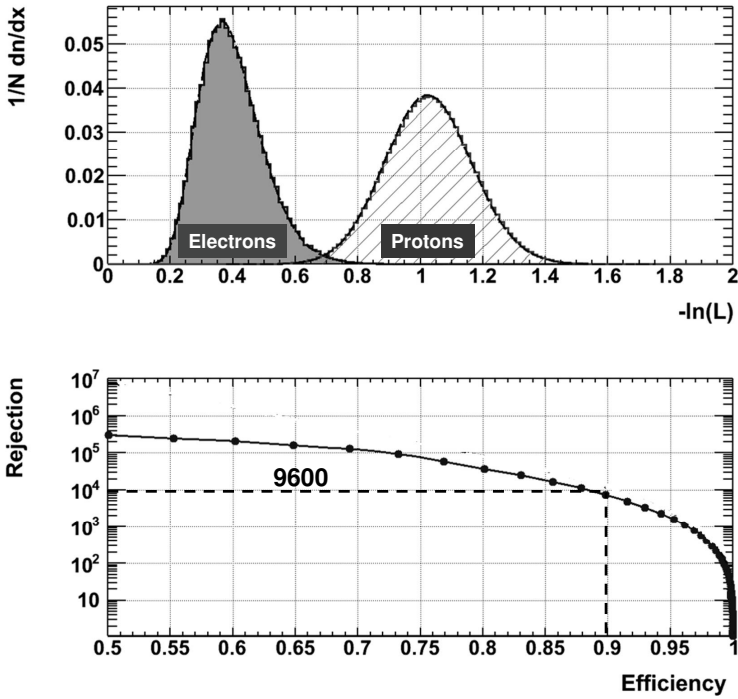


Fig. 18. The upper plot shows the separation power of the TRD log likelihood estimator in the energy range 3–100 GeV (ISS data). The lower plot shows that at 90% of electron/positron efficiency the measured proton rejection is 1/9600 over the energy range 3–100 GeV.

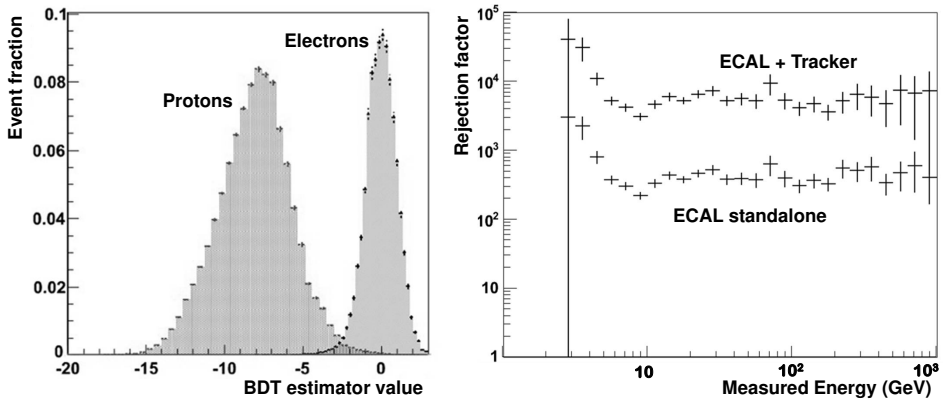


Fig. 19. The left plot shows the separation power of the ECAL estimator in the energy range 3–1000 GeV (ISS data). The right plot shows that at 90% of electron/positron efficiency the measured proton rejection is $\sim 1/400$ for ECAL only, and $\sim 1/5000$ for the combination of the ECAL and the tracker over the energy range 3–1000 GeV.

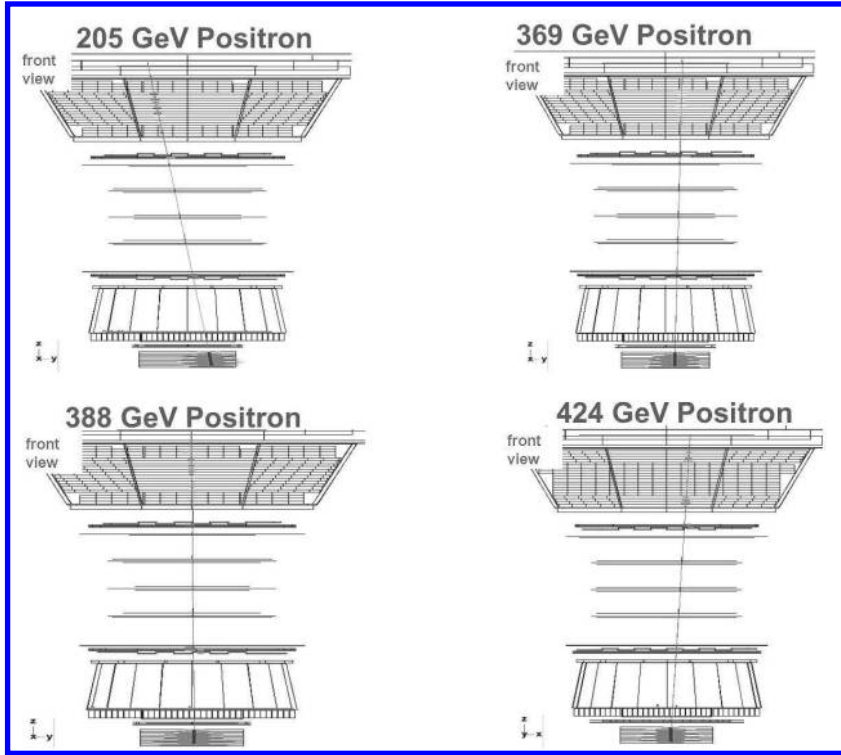


Fig. 20. Examples of high energy positrons detected by AMS.

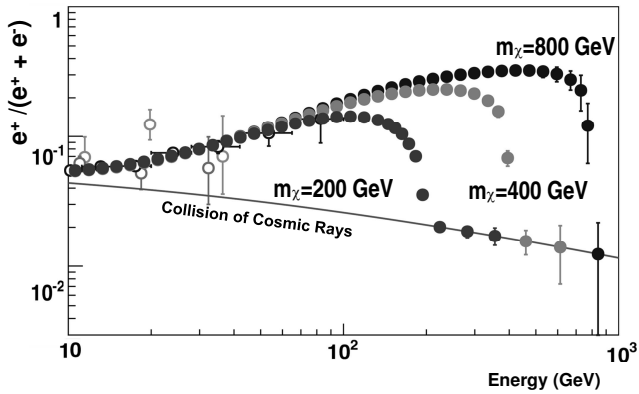


Fig. 21. Dependence of the expected positron spectrum shape on the neutralino mass. Open circles with large error bars correspond to the compilation of the available measurements^{19–22} from AMS-01, HEAT and PAMELA. Full circles of different shading correspond to the signal expected in AMS-02 from neutralinos of 200, 400 and 800 GeV assuming 18 years of collecting data.

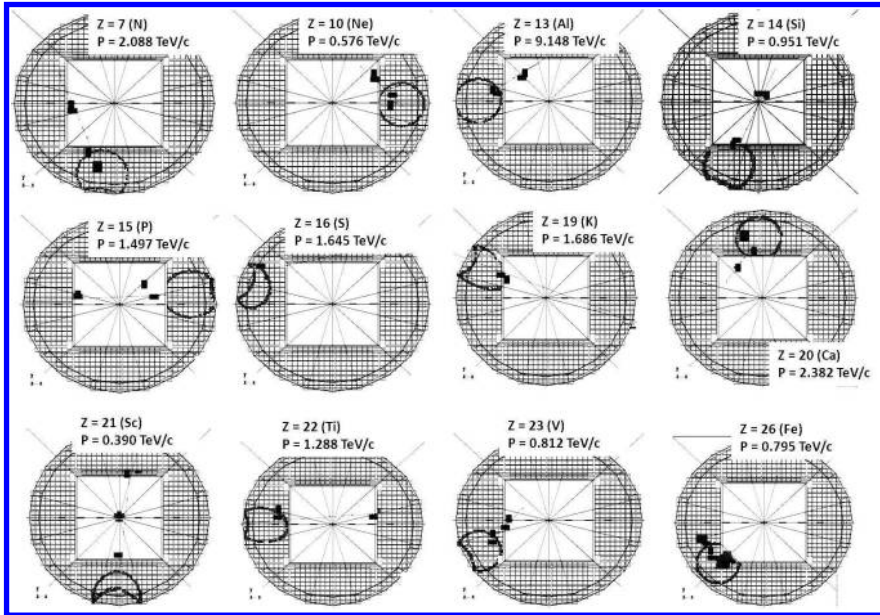


Fig. 22. Examples of nuclei with momenta in TeV range detected by AMS.

It should be noted that three-dimensional shower reconstruction in the ECAL provides an accurate estimate of the direction and coordinates. The reconstructed shower axis can be traced back to match with the information from other detectors. For electron and positron candidates there are matching traces in the TRD, TOF and tracker, for photon candidates these matching traces in other detectors are absent.

5.2. Search for primordial anti-matter

Conditions that are required for the baryon asymmetry in the Universe have no experimental support. To date neither strong CP-violation nor proton decay have been observed. Therefore, despite being disfavored,³⁸ large anti-matter domains in the Universe may not be ruled out *a priori*.³⁹ Also, small pockets of primordial anti-matter are not excluded.⁴⁰ Such pockets or domains, if they exist, would emit anti-matter nuclei which will eventually reach Earth through a diffusion process. Production of anti-helium or heavier anti-nuclei in the interaction of ordinary matter in space is totally negligible; therefore the observation of a single anti-helium nuclei in space would constitute a strong argument in favor of such anti-matter domains.

Examples of collected $Z > 1$ particles are shown in Fig. 22. The radius of the RICH rings measure the velocity of the particles (redundant measurements are performed using also the TOF and the tracker). The number of photoelectrons in

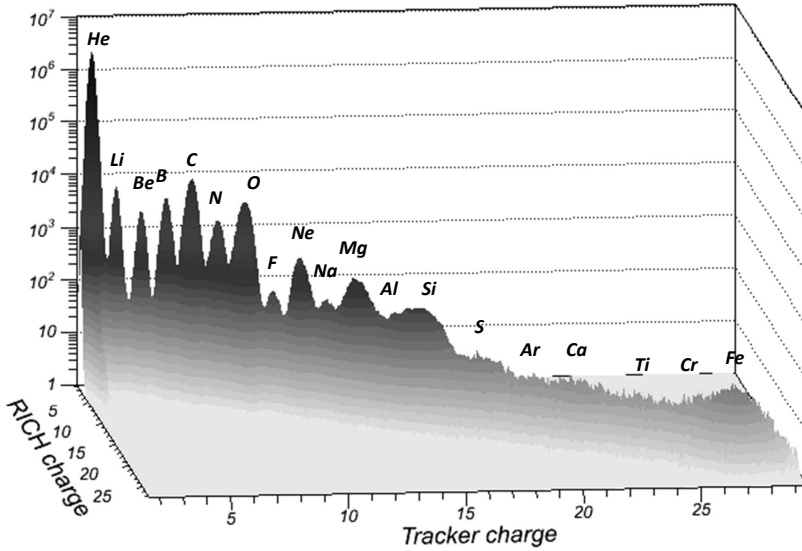


Fig. 23. Correlation of simultaneous charge measurements in the RICH and the tracker.

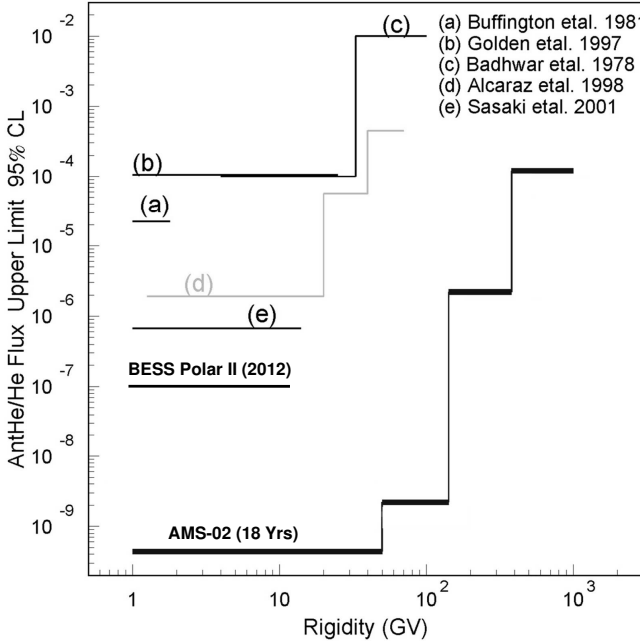


Fig. 24. Expected sensitivity of AMS for 18 years of data taking on the ISS compared with the available measurements. Recent 2012 results from BESS⁴² are also shown.

the ring determines the charge (redundant measurements of the absolute charge value are also done by the TRD, the TOF and the tracker). Presented in Fig. 23 is the determination of cosmic ray relative nuclear abundances as measured by the RICH and the tracker.

One of the goals of AMS is to improve the sensitivity of a direct anti-matter search by 3 to 6 orders of magnitude (depending on the energy range) and increase the current search range to 1 TeV. This is demonstrated in Fig. 24 where expected sensitivity of AMS with the available measurements. Results presented in this figure use no assumption that He and anti-He spectra are identical.

5.3. Search for exotic forms of matter

AMS represents an unprecedented opportunity to explore the unknown. One example is the search for new types of matter such as strangelets.⁴¹ Strangelets, or strange quark matter (SQM), are new types of matter composed of three types of quarks (u, d, s) which may exist in the cosmos. Both lattice QCD and phenomenological bag model calculations indicate that SQM could be stable with lower energy levels than usual matter. SQM has a very low Z/A ratio, typically less than 0.13 compared to the ~ 0.5 of normal nuclei. Attempts to detect SQM production in accelerators are negative, which agrees with calculations that indicate they cannot be formed there by coalescence nor distillation (the minimum stable size, $A > 8$, is too large). Neutron stars could in fact be one large strangelet at low vapor pressure, providing a source of SQM in cosmic rays. Searches for SQM on Earth and in lunar samples are negative but of limited sensitivity (e.g., large strangelets are so dense they would sink to the center of gravity). AMS-01 has observed a potential strangelet candidate with $Z = 2$ and a mass of 16.5 GeV, with the estimated flux of 5×10^{-5} (sr m² s)⁻¹. AMS-02 will provide much improved sensitivity for the search of this new type of matter.

6. Conclusions

AMS has involved over 17 years of effort by hundreds of scientists, engineers and students from all over the world. Many government agencies in the United States, Europe and Asia have strongly supported AMS and many have considered AMS a national priority. It is because of the scientific merit of AMS, but also the dedication and hard work of many people, in many walks of life, that AMS is a reality.

The primary motivation of AMS is to explore the unknown realm of space where answers to many of the most fundamental questions in physics, astrophysics and cosmology may be definitively answered. It is a unique opportunity to make major discoveries and advancements in our understanding of the universe that cannot be done on Earth.

At present ISS operations are approved till 2020 and intensive discussions are continuing between the ISS space agencies to certify the onboard elements through 2028. These discussions are further stimulated by a significant enhancement of the

ISS scientific program with the deployment of AMS-02 onboard ISS. Therefore, at this time, we assume that AMS-02 will collect data over 18 years. Given the unprecedented statistical significance of the AMS-02 data sample, the AMS collaboration is now fully focused on the analysis of the data. The highest priority is given to the in-depth understanding of the detector behavior in order to maximize the accuracy of the physics measurements.

Acknowledgments

AMS was begun by Professor Samuel Ting of the Massachusetts Institute of Technology. At present this is a collaboration of 600 physicists from 60 universities and research institutes from 16 countries. Figure 25 illustrates the worldwide scope of the AMS collaboration.

Since the beginning, AMS has been strongly and continuously supported by the MIT School of Science and the Laboratory for Nuclear Science. In 1994, the leadership of NASA recognized the scientific value of AMS in providing major science to the International Space Station. We thank former NASA Administrator Mr. Daniel S. Goldin for his dedication to the legacy of the ISS as an important scientific laboratory and his decision for NASA to fly AMS as a U.S. Department of Energy (DOE) sponsored payload. We also thank Mr. George Abbey for his insight and encouragement. We also acknowledge the strong and continuous support of the NASA Administrator General Charles Bolden and Deputy Administrator Lori Garver.

AMS is a DOE sponsored international collaboration. We are grateful to the strong and continuous support of the Office of Science, division of High Energy Physics for their leadership and strong support to AMS. The rigorous reviews conducted by DOE and by other funding agencies, along with their strong and continuous support over the last 17 years, have made AMS a reality.

We acknowledge with appreciation the support of Parliamentary State Secretary in the Federal Ministry of Economics and Technology of the Republic of Germany, Mr. Peter Hintze, the Speaker of the French Parliament, Dr. Bernard Accoyer, former President of Academia Sinica (Taiwan) and Nobel Laureate Professor Y.T. Lee and Minister of Science of Taiwan, Academician Lou-Chuang Lee.

The major components of AMS were constructed in the U.S., Italy, Germany, Taiwan, Spain, France, Switzerland, China and the Netherlands. We are grateful to the many universities and government funding agencies in AMS for their support.

In particular, we acknowledge the strong support from: IN2P3 (France); DLR and RWTH-Aachen (Germany), ASI and INFN (Italy), the Swiss National Science Foundation, FIT Zurich and the University of Geneva (Switzerland), CIEMAT, CDTI and the National Research Plan (Spain), the Academy of Sciences, MOST, NLAA, and the Provincial Governments of Shandong, Jiangsu, and Guandong (China) and the Academia Sinica, the National Science Council and CSIST (Taiwan).

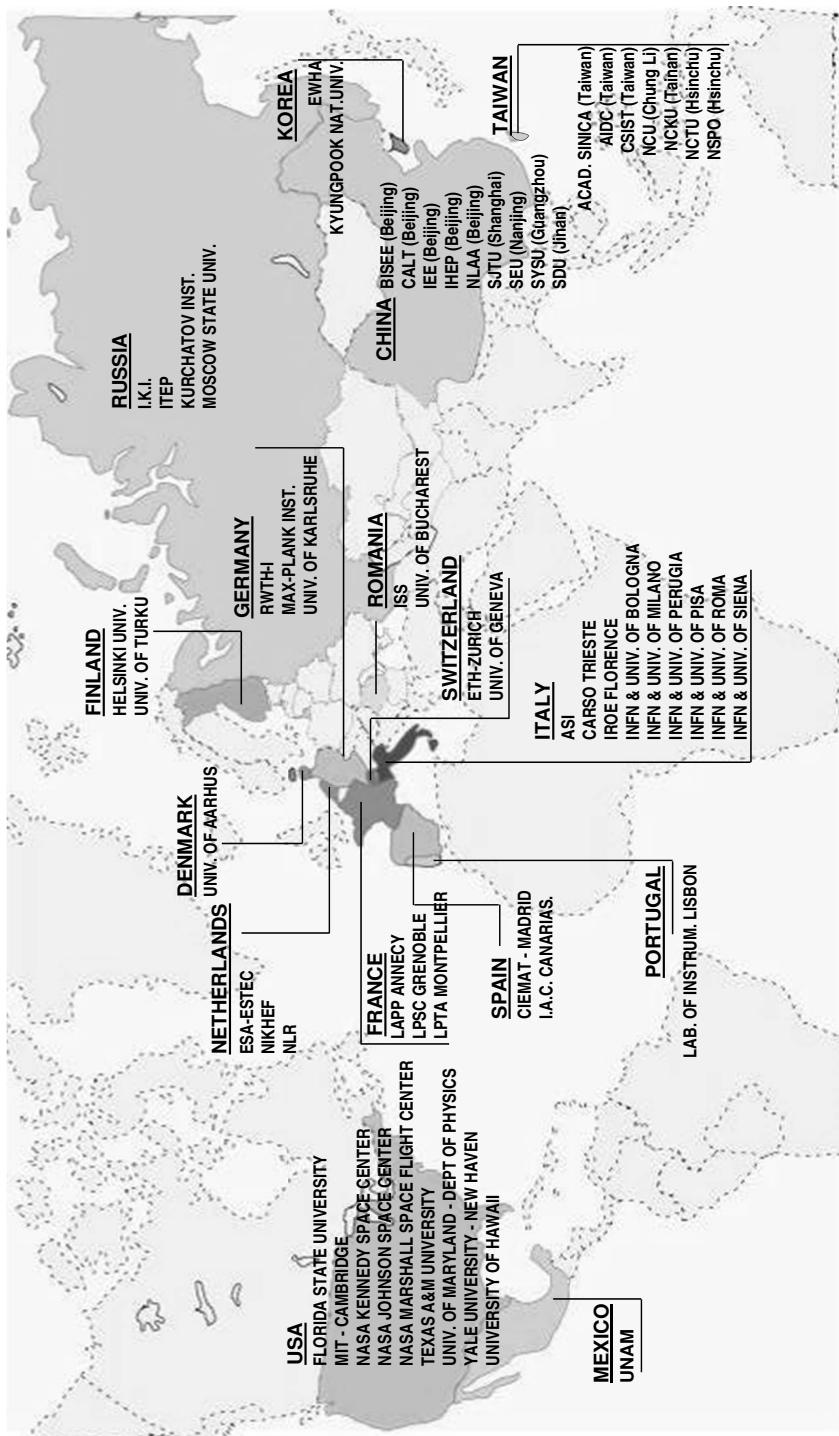


Fig. 25. The AMS Collaboration includes 60 universities and research institutes from 16 countries.

The European Center for Nuclear Research (CERN) and the European Space Agency have provided most valued support to AMS in providing assembly and testing facilities. These have included repeated tests in the accelerator beam at CERN and EMC and TVT tests at ESTEC in Holland. We extend our deepest thanks to Professor Rolf-Dieter Heuer (Director General of CERN), and Professor Jean Jacques Dordain (Director of the European Space Agency) and Dr. Simona DiPippo (Director of Human Space Flight, European Space Agency) for their outstanding leadership and support. We also thank former Director General of CERN (Professor Luciano Maiani and Dr. Robert Aymar) for the important part they played in supporting AMS activities at CERN.

We especially thank Mr. William Gerstenmeier, NASA Associate Administrator for Human Space Flight, for his enduring support and encouragement. His conviction that the ISS be utilized for fundamental science has been an inspiration to the Collaboration. We are grateful to the NASA Johnson Space Center AMS Project Management Office under Mr. Trent Martin and Mr. Ken Bollweg for expert guidance and support and especially for working closely with us through the challenges of bringing experimental particle physics to space.

We thank Nobel Laureates Steven Weinberg, James Cronin and George Smoot, Members of the U.S. National Academy of Sciences; Professor Len Fisk, Professor Barry Barish; and Professor Neal Lane, former Presidential Science Advisor and Professor Jonathan Ellis, Fellow of the Royal Society (U.K.) for many significant discussions of great importance to AMS.

Finally, we acknowledge with profound appreciation the United States Congress for their unanimous approval of HR6063 (2008) which mandated the addition of this shuttle flight (STS-134) for AMS. We particularly thank the late Senator Ted Stevens, Senator Daniel K. Inouye, Senator Kay Bailey Hutchison, Senator Bill Nelson, Senator David Vitter, Congressman Ralph Hall, Congressman Joe Barton, Congresswoman Gabrielle Giffords, former Congressman Nick Lampson, former Senator and Astronaut John Glenn and Senior Senate Advisor, Mr. Jeff Bingham for their critical support. Their understanding of the value of fundamental scientific research and international collaboration restored AMS to the shuttle manifest and gave Endeavor one final mission to bring major science to the ISS.

References

1. M. Garcia-Munoz, G. Mason and J. Simpson, *Astrophys. J.* **202** (1975) 265.
2. M. Garcia-Munoz, G. Mason and J. Simpson, *Astrophys. J.* **217** (1977) 859.
3. W. R. Binns *et al.*, *Astrophys. J.* **324** (1988) 1106.
4. J. Engelmann *et al.*, *Astron. Astrophys.* **233** (1990) 96.
5. A. Labrador *et al.*, *Proc. 28th Int. Cosmic Ray Conference* (Tsukuba, Japan, 2003), p. 1773.
6. R. C. Hartman *et al.*, *Astrophys. J. Suppl.* **123** (1999) 79.
7. B. Atwood *et al.*, *Asptrophys. J.* **697** (2009) 1071.
8. O. Adriani *et al.*, *AIP Conf. Proc.* **1223** (2010) 33.
9. J. Carson, *J. Phys. Conf. Ser.* **60** (2007) 115.

10. M. Aguilar *et al.*, *Phys. Rep.* **366/6** (2002) 331.
11. A. Yamamoto *et al.*, *Adv. Space Res.* **14/2** (1994) 75.
12. W. Menn *et al.*, *Asptrophys. J.* **553** (2000) 281.
13. S. W. Barwick *et al.*, *Asptrophys. J.* **498** (1998) 779.
14. S. Coutu *et al.*, *Astropart. Phys.* **11** (1999) 429.
15. P. Panini *et al.*, *Asptrophys. J.* **615** (2004) 259.
16. G. Grimani *et al.*, *Asptrophys. J.* **392** (2002) 287.
17. R. M. Baltrusaitis *et al.*, *Nucl. Instrum. Meth. A* **240** (1985) 410.
18. J. Abraham *et al.*, *Nucl. Instrum. Meth. A* **523** (2004) 50.
19. S. W. Berwick *et al.*, *Astrophys. J.* **482** (1997) 191.
20. M. Aguilar *et al.*, *Phys. Lett. B* **646** (2007) 145.
21. O. Adriani *et al.*, *Nature* **458** (2009) 607.
22. M. Ackermann *et al.*, *Phys. Rev. Lett.* **108** (2012) 011103.
23. J. Alcaraz *et al.*, *Phys. Lett. B* **461** (1999) 387.
24. J. Alcaraz *et al.*, *Phys. Lett. B* **472** (2000) 215.
25. J. Alcaraz *et al.*, *Phys. Lett. B* **484** (2000) 10.
26. J. Alcaraz *et al.*, *Phys. Lett. B* **490** (2000) 27.
27. J. Alcaraz *et al.*, *Phys. Lett. B* **494** (1999) 193.
28. M. Aguilar *et al.*, *Phys. Lett. B* **646** (2007) 145.
29. Ph. Doetinchem *et al.*, *Nucl. Instrum. Meth. A* **558** (2006) 526.
30. D. Alvisi *et al.*, *Nucl. Instrum. Meth. A* **437** (1999) 212.
31. Ph. Doetinchem *et al.*, *Nucl. Phys. B* **197** (2009) 15.
32. J. Alcaraz *et al.*, *Nucl. Instrum. Meth. A* **593** 376.
33. J. Casaus, *Nucl. Phys. B Proc. Suppl.* **113** (2002) 147.
34. F. Cadoux *et al.*, *Nucl. Phys. B Proc. Suppl.* **113** (2002) 159.
35. W. W. Peterson and D. T. Brown, *Proc. IRE* **49** (1961) 228.
36. D. A. Huffman, *Proc. IRE* **40** (1952) 1098.
37. G. Jungman, M. Kamionkovski and K. Griest, *Phys. Rep.* **267** (1996) 195.
38. A. G. Cohen, A. DeRujula and S. L. Glashow, *Astrophys. J.* **495** (1998) 539.
39. Y. B. Zeldovich, I. Y. Kobzarev and L. B. Okun, *J. Exp. Theor. Phys.* **40** (1974) 1.
40. M. Y. Khlopov, S. G. Rubin and A. S. Sakharov, *Phys. Rev. D* **62** (2000) 083505.
41. E. Witten, *Phys. Rev. D* **30** (1984) 272.
42. K. Abe *et al.*, arXiv:1201.2967v1.

This article has been cited by:

1. S. Scopel, N. Fornengo, A. Bottino. 2013. Embedding the 125 GeV Higgs boson measured at the LHC in an effective MSSM: Possible implications for neutralino dark matter. *Physical Review D* **88**:2. . [[CrossRef](#)]
2. C. Pizzolotto. 2013. AMS-02 after one year in space. *Nuclear Physics B - Proceedings Supplements* **239-240**, 135-139. [[CrossRef](#)]
3. M. Aguilar, G. Alberti, B. Alpat, A. Alvino, G. Ambrosi, K. Andeen, H. Anderhub, L. Arruda, P. Azzarello, A. Bachlechner, F. Barao, B. Baret, A. Barrau, L. Barrin, A. Bartoloni, L. Basara, A. Basili, L. Batalha, J. Bates, R. Battiston, J. Bazo, R. Becker, U. Becker, M. Behlmann, B. Beischer, J. Berdugo, P. Berges, B. Bertucci, G. Bigongiari, A. Biland, V. Bindi, S. Bizzaglia, G. Boella, W. de Boer, K. Bollweg, J. Bolmont, B. Borgia, S. Borsini, M. J. Boschini, G. Boudoul, M. Bourquin, P. Brun, M. Buénerd, J. Burger, W. Burger, F. Cadoux, X. D. Cai, M. Capell, D. Casadei, J. Casaus, V. Cascioli, G. Castellini, I. Cernuda, F. Cervelli, M. J. Chae, Y. H. Chang, A. I. Chen, C. R. Chen, H. Chen, G. M. Cheng, H. S. Chen, L. Cheng, N. Chernoplyokov, A. Chikanian, E. Choumilov, V. Choutko, C. H. Chung, C. Clark, R. Clavero, G. Coignet, V. Commichau, C. Consolandi, A. Contin, C. Corti, M. T. Costado Dios, B. Coste, D. Crespo, Z. Cui, M. Dai, C. Delgado, S. Della Torre, B. Demirkoz, P. Dennett, L. Derome, S. Di Falco, X. H. Diao, A. Diago, L. Djambazov, C. Díaz, P. von Doetinchem, W. J. Du, J. M. Dubois, R. Duperay, M. Duranti, D. D'Urso, A. Egorov, A. Eline, F. J. Eppling, T. Eronen, J. van Es, H. Esser, A. Falvard, E. Fiandrini, A. Fiasson, E. Finch, P. Fisher, K. Flood, R. Foglio, M. Fohey, S. Fopp, N. Fouque, Y. Galaktionov, M. Gallilee, L. Gallin-Martel, G. Gallucci, B. García, J. García, R. García-López, L. García-Tabares, C. Gargiulo, H. Gast, I. Gebauer, S. Gentile, M. Gervasi, W. Gillard, F. Giovacchini, L. Girard, P. Goglov, J. Gong, C. Goy-Henningsen, D. Grandi, M. Graziani, A. Grechko, A. Gross, I. Guerri, C. de la Guía, K. H. Guo, M. Habiby, S. Haino, F. Hauler, Z. H. He, M. Heil, J. Heilig, R. Hermel, H. Hofer, Z. C. Huang, W. Hungerford, M. Incagli, M. Ionica, A. Jacholkowska, W. Y. Jang, H. Jinchu, M. Jongmanns, L. Journet, L. Jungermann, W. Karpinski, G. N. Kim, K. S. Kim, Th. Kirn, R. Kossakowski, A. Koulemzine, O. Kounina, A. Kounine, V. Koutsenko, M. S. Krafczyk, E. Laudi, G. Laurenti, C. Lauritzen, A. Lebedev, M. W. Lee, S. C. Lee, C. Leluc, H. León Vargas, V. Lepareur, J. Q. Li, Q. Li, T. X. Li, W. Li, Z. H. Li, P. Lipari, C. H. Lin, D. Liu, H. Liu, T. Lomtadze, Y. S. Lu, S. Lucidi, K. Lübelmeyer, J. Z. Luo, W. Lustermann, S. Lv, J. Madsen, R. Majka, A. Malinin, C. Mañá, J. Marín, T. Martin, G. Martínez, F. Masciocchi, N. Masi, D. Maurin, A. McInturff, P. McIntyre, A. Menchaca-Rocha, Q. Meng, M. Menichelli, I. Mereu, M. Millinger, D. C. Mo, M. Molina, P. Mott, A. Mujunen, S. Natale, P. Nemeth, J. Q. Ni, N. Nikonov, F. Nozzoli, P. Nunes, A. Obermeier, S. Oh, A. Oliva, F. Palmonari, C. Palomares, M. Panicia, A. Papi, W. H. Park, M. Pauluzzi, F. Pauss, A. Pauw, E. Pedreschi, S. Pensotti, R. Pereira, E. Perrin, G. Pessina, G. Pierschel, F. Pilo, A. Piluso, C. Pizzolotto, V. Plyaskin, J. Pochon, M. Pohl, V. Poireau, S. Porter, J. Poux, A. Putze, L. Quadrani, X. N. Qi, P. G. Rancoita, D. Rapin, Z. L. Ren, J. S. Ricol, E. Riihonen, I. Rodríguez, U. Roeser, S. Rosier-Lees, L. Rossi, A. Rozhkov, D. Rozza, A. Sabellek, R. Sagdeev, J. Sandweiss, B. Santos, P. Saouter, M. Sarchioni, S. Schael, D. Schinzel, M. Schmanau, G. Schwering, A. Schulz von Dratzig, G. Scolieri, E. S. Seo, B. S. Shan, J. Y. Shi, Y. M. Shi, T. Siedenburger, R. Siedling, D. Son, F. Spada, F. Spinella, M. Steuer, K. Stiff, W. Sun, W. H. Sun, X. H. Sun, M. Tacconi, C. P. Tang, X. W. Tang, Z. C. Tang, L. Tao, J. Tassan-Viol, Samuel C. C. Ting, S. M. Ting, C. Titus, N. Tomassetti, F. Toral, J. Torsti, J. R. Tsai, J. C. Tutt, J. Ulbricht, T. Urban, V. Vagelli, E. Valente, C. Vannini, E. Valtonen, M. Vargas Trevino, S. Vaurynovich, M. Vecchi, M. Vergain,

B. Verlaet, C. Vescovi, J. P. Vialle, G. Viertel, G. Volpini, D. Wang, N. H. Wang, Q. L. Wang, R. S. Wang, X. Wang, Z. X. Wang, W. Wallraff, Z. L. Weng, M. Willenbrock, M. Wlochal, H. Wu, K. Y. Wu, Z. S. Wu, W. J. Xiao, S. Xie, R. Q. Xiong, G. M. Xin, N. S. Xu, W. Xu, Q. Yan, J. Yang, M. Yang, Q. H. Ye, H. Yi, Y. J. Yu, Z. Q. Yu, S. Zeissler, J. G. Zhang, Z. Zhang, M. M. Zhang, Z. M. Zheng, H. L. Zhuang, V. Zhukov, A. Zichichi, P. Zuccon, C. Zurbach. 2013. First Result from the Alpha Magnetic Spectrometer on the International Space Station: Precision Measurement of the Positron Fraction in Primary Cosmic Rays of 0.5–350 GeV. *Physical Review Letters* **110**:14. . [[CrossRef](#)]